IOP Publishing Modelling and Simulation in Materials Science and Engineering

Modelling Simul. Mater. Sci. Eng. **24** (2016) 035015 (13pp) doi:10.1088/0965-0393/24/3/035015

A Markov random field approach for microstructure synthesis

A Kumar[2], L Nguyen[3], M DeGraef[3] and V Sundararaghavan[1]

[1] Aerospace Engineering, University of Michigan, Ann Arbor, MI, USA
[2] Oak Ridge National Lab, Oak Ridge, TN, USA
[3] Materials Science and Engineering, Carnegie Mellon University, PA 15213, USA

E-mail: veeras@umich.edu

Received 4 April 2015, revised 2 December 2015
Accepted for publication 22 January 2016
Published 8 March 2016

Abstract

We test the notion that many microstructures have an underlying stationary probability distribution. The stationary probability distribution is ubiquitous: we know that different windows taken from a polycrystalline microstructure are generally 'statistically similar'. To enable computation of such a probability distribution, microstructures are represented in the form of undirected probabilistic graphs called Markov Random Fields (MRFs). In the model, pixels take up integer or vector states and interact with multiple neighbors over a window. Using this lattice structure, algorithms are developed to sample the conditional probability density for the state of each pixel given the known states of its neighboring pixels. The sampling is performed using reference experimental images. 2D microstructures are artificially synthesized using the sampled probabilities. Statistical features such as grain size distribution and autocorrelation functions closely match with those of the experimental images. The mechanical properties of the synthesized microstructures were computed using the finite element method and were also found to match the experimental values.

Keywords: reconstruction, microstructure, finite element analysis, simulation, probability

(Some figures may appear in colour only in the online journal)

1. Introduction

Microstructures are stochastic in nature and a single snapshot of the microstructure does not give its complete variability. However, we know that different windows taken from a polycrystalline microstructure generally 'look alike'. In mathematical terms, this amounts to the presence of a stationary probability distribution from which various microstructural snapshots are

sampled. There are various ways of modeling this probability distribution indirectly. Feature-based algorithms have long been used that categorize various microstructural snapshots based on a common set of underlying features, and generate new synthetic images with similar features [1–3]. These features could include marginal histograms [1], multiresolution filter outputs (Gaussian [2] and wavelet [3] filters) and point probability functions (e.g. autocorrelation function) [4]. These methods are good at capturing the global features (volume averaged) of the image, however local geometric geometric features are not reconstructed correctly. Thus, features such as grain boundaries are smeared out when reconstructing polycrystalline structures [3]. Reconstruction of heterogeneous material such as geological materials [5], and particulate materials [6] are also performed using techniques similar to polycrystalline materials.

Alternatively, one could start with sampling the conditional probability density for the state of a pixel given the known states of its neighboring pixels [7–10] using reference 2D or 3D experimental images. If only the nearest neighbors are chosen, this amounts to sampling from a Ising-type model [11, 12]. For general microstructures, the correlation lengths can span several pixels and a larger neighbor window may be needed [4]. In this work, we employ generalized Ising models called Markov Random Fields (MRFs) to model the probability distribution. While in Ising models, a lattice is constructed with pixels (with binary states) interacting with its nearest neighbors, in MRFs, pixels take up integer or vector states and interact with multiple neighbors over a window. The sampling of conditional probability of a pixel given the states of its known neighbors is based on Claude Shannon's generalized Markov chain [13]. In the one dimensional problem, a set of consecutive pixels is used as a template to determine the probability distribution function (PDF) of the next pixel. Sundararaghavan [14] used this approach for synthesizing 3D microstructures from 2D micrographs. Here, pixel variables in a 3D microstructure were optimized so as to match the conditional probability densities on orthogonal 2D sections with the reference images. In this work, an alternate approach is employed where microstructures are grown layer-by-layer from a small seed image (3×3 pixels) taken randomly from the experimental micrograph. The algorithm first finds all windows in an experimental micrograph that are similar to an unknown pixel's neighborhood window. One of these matching windows is chosen and its center pixel is taken to be the newly synthesized pixel.

We use this method to generate polycrystalline microstructures. Voronoi construction has been typically used for the synthesis of such microstructures [15–18]. However, Voronoi constructions are largely an idealization and do not account for the complexity of real microstructures (e.g. non-convex grain shapes). A MRF algorithm can be an attractive replacement for these models as it captures fine scale structure such as grain boundaries realistically. In this paper, we test the synthetic microstructures generated by this method by comparing its statistical measures including lower order statistics (e.g. grain size distribution, orientation distribution function) and finer features (e.g. shape moment invariants, autocorrelation function) with those of experimental images. In addition, physical properties such as elastic moduli and stress distribution are also calculated using image-based finite element models and compared against experiments. The results are discussed in section 3.

2. Mathematical modeling of microstructures as Markov random fields

Some of early attempts at microstructure modeling were based on Ising models [11]. In the Ising model, a $N \times N$ lattice (L) is constructed with values X_i assigned for each particle i on the lattice, $i \in [1, .., N^2]$. In an Ising model, X_i is a binary variable equal to either $+1$ or -1 (e.g. magnetic moment [11]). In this work, the values X_i may contain any one of G color levels in

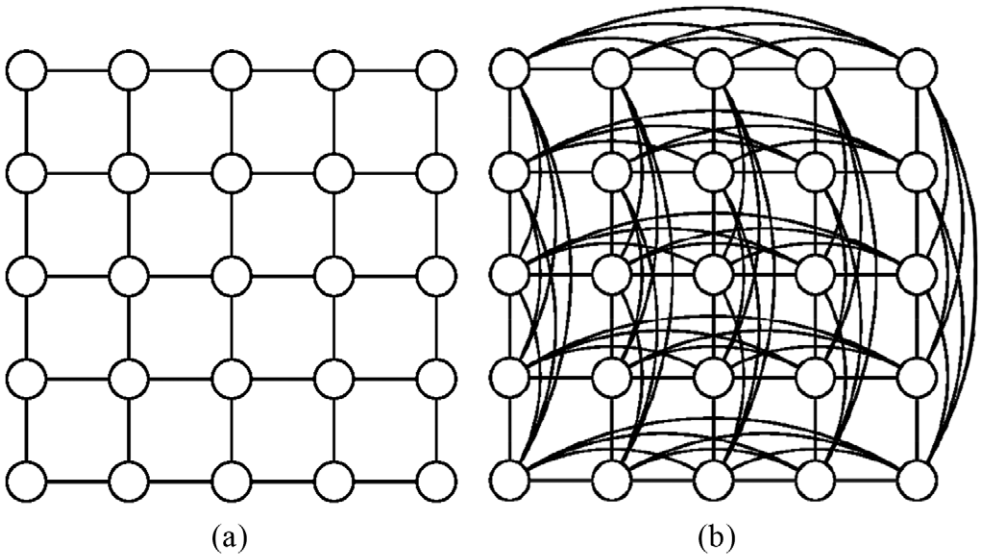

Figure 1. Markov random field as an undirected graph model, circles are pixels in the image and bonds are used to connect neighbors: (a) Ising model with nearest neighbor interactions (b) microstructure modeled by including higher order interactions in the Ising model.

the range $\{0, 1, .., G-1\}$ (following the integer range extension of the Ising model by Besag [19]). A *coloring* of L denoted by $\boldsymbol{X}$ maps each particle in the lattice L to a particular value in the set $\{0, 1, .., G-1\}$. Ising models fall under the umbrella of *undirected graph models* in probability theory. In order to rewrite the Ising model as a graph, we assign neighbors to particles and link pairs of neighbors using a bond as shown in figure 1(a). The rule to assign neighbors is based on a *pairwise Markov property*. A particle j is said to be a neighbor of particle i only if the conditional probability of the value X_i given all other particles (except (i, j), i.e. $p(X_i|X_1, X_2, .., X_{i-1}, X_{i+1}, .., X_{j-1}, X_{j+1}, .., X_{N^2})$) depends on the value X_j.

Note that the above definition does not warrant the neighbor particles to be close in distance, although this is widely employed for physical reasons. For example, in the classical Ising model, each particle is bonded to the next nearest neighbor as shown in figure 1(a). In this work, we assume that a microstructure is a higher order Ising model (figure 1(b)). The particles of the microstructure correspond to pixels of the 2D image. The neighborhood of a pixel is modeled using a square window around that pixel and bonding the center pixel to every other pixel within the window. Using this graph structure, a *Markov random field* can be defined as the joint probability density $P(\boldsymbol{X})$ on the set of all possible colorings $\boldsymbol{X}$, subject to a *local Markov property*. The *local Markov property* states that the probability of value X_i, given its neighbors, is conditionally independent of the values at all other particles. In other words, $P(X_i|\text{all particles except } i) = p(X_i|\text{neighbors of particle } i)$. Next, we describe a method based on [10] to sample from the conditional probability density $p(X_i|\text{neighbors of voxel } i)$.

2.1. Sampling algorithm

In the following discussion, the color (X_i) of a pixel i is represented using G color levels in the range $\{0, 1, .., G-1\}$ each of which maps to an RGB triplet. The number of color levels is

chosen based on the microstructure to be reconstructed, e.g. for binary images $G = 2$. Let $\boldsymbol{E}$ and $\boldsymbol{S}$ denote the experimental and synthesized microstructure, respectively. Let v be a pixel in $\boldsymbol{S}$ whose color needs to inferred using the sampling procedure. Let $\boldsymbol{S}_v$ denote the colors in a neighborhood window around pixel v. Let $\boldsymbol{E}^w$ denote the colors of pixels in a window of the same size in the input 2D micrograph.

In order to find the coloring of pixel v, one needs to compute the conditional probability density $p(X_v|\boldsymbol{S}_v)$. Explicit construction of such a probability density is often computationally intractable. Instead, the most likely value of v is identified by first finding a window $\boldsymbol{E}^{w*}$ in the input 2D micrograph that is most similar to $\boldsymbol{S}_v$ (see figure 1). This is done by solving the following problem (where $\boldsymbol{S}_{v,u}$ denotes the color of pixel u in $\boldsymbol{S}_v$ and $\boldsymbol{E}^w_u$ denotes the color of pixel u in $\boldsymbol{E}^w$):

$$\begin{aligned} \boldsymbol{E}^{w*} &= \arg\min_{\boldsymbol{E}^w} D \\ \text{where, } D &= \sum_u \omega_u \|\boldsymbol{S}_{v,u} - \boldsymbol{E}^w_u\|^2 \end{aligned} \tag{1}$$

In the above equation, D is a distance measure defined as the normalized sum of weighted squared differences of pixel colors. The weights for nearby pixels are taken to be greater than for pixels farther away based on a Gaussian weighting function (ω). If the pixel u is located at position (x, y) (in lattice units) with respect to the center pixel (located at $(0, 0)$), ω_u is given as:

$$\omega_u = \frac{\exp(-\frac{(x^2+y^2)}{2\sigma^2})}{\sum_i \sum_j \exp(-\frac{(i^2+j^2)}{2\sigma^2})} \tag{2}$$

Here, the summation in the denominator is taken over all the known pixels in $\boldsymbol{S}_v$. The weights ω_u for the unknown pixels in $\boldsymbol{S}_v$ are taken to be zero. This ensures that the distance measure is computed only using the known values and is normalized by the total number of known pixels. The standard deviation (σ) is taken to be 0.16.

The problem in equation (1) is solved using an exhaustive search by comparing all the windows in the input 2D micrograph to the corresponding neighborhood of pixel v. In our approach, a measure of stochasticity is introduced by storing all matches with a distance measure that is within 1.3 times that of the best matching window [10]. The center pixel colors of all these matches give a histogram for the color of the unknown pixel (X_v), which is then sampled using a uniform random number.

The microstructure is grown layer-by-layer starting from a small seed image (3×3 pixels) taken randomly from the experimental micrograph (figure 2). In this way, for any pixel the values of only some of its neighborhood pixels will be known. The fundamental approximation in this numerical implementation is that the probability distribution function (PDF) of an unfilled pixel is assumed to be independent of the PDF of its unfilled neighbors. Each iteration in the algorithm involves coloring the unfilled pixels along the boundary of filled pixels in the synthesized image as shown in figure 2. An upper limit of 0.1 is enforced for the distance measure initially. If the matching window for a unfilled pixel has a larger distance measure, then the pixel is temporarily skipped while the other pixels on the boundary are filled. If none of the pixels on the boundary can be filled during an iteration, then the threshold is increased by 10% for the next iteration.

Although there are several free parameters in this model, we choose the window size to be the only adjustable parameter for different microstructures for simplicity. Window size plays an important role in the MRF model. At window sizes much smaller than the correlation lengths, false matches lead to high noise in the reconstructions. At very high window sizes, not

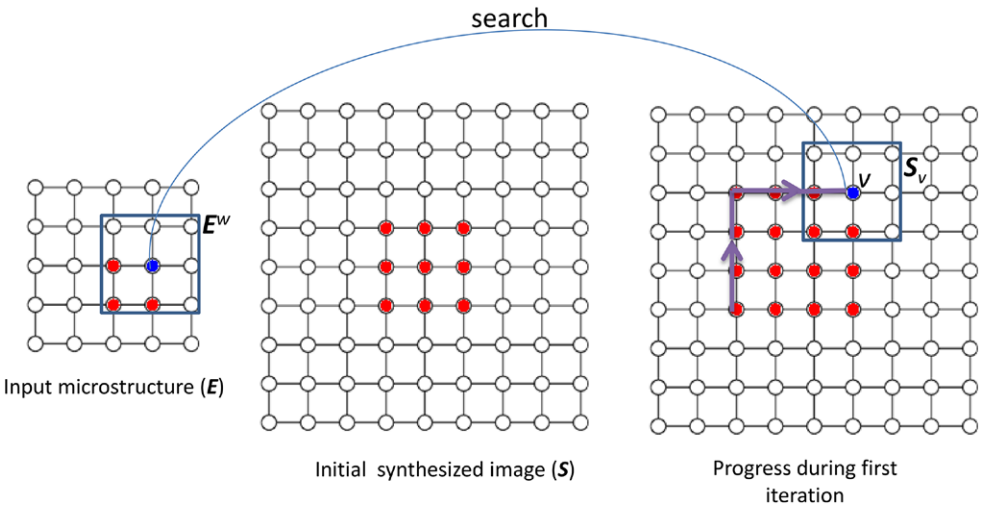

Figure 2. The Markov random field approach [10, 20]: The image is grown from a 3×3 seed image (center). As the algorithm progresses along the path shown (right), the unknown output pixel (shown in blue) is computed by searching for a pixel with a similar neighborhood in the input image (left).

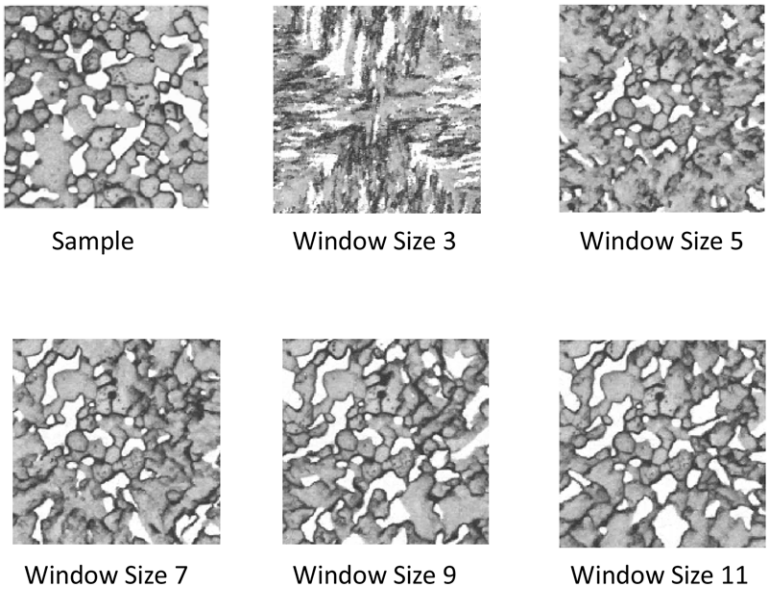

Figure 3. Effect of Window size, none of the image looks similar to sample image but image generated with window size of 11 has statistical correlation function very much similar to that of sample image.

enough matching windows can be identified. Hence, there is an ideal window size that needs to be found through numerical trial. In figure 3 we have demonstrated the effect of window size on quality of synthesized image. Note that only odd values were allowed for the window size so that the window is symmetric around the center pixel. This example is of a two phase W-Ag composite from [21].

3. Examples

In order to test the physical features and properties of the synthesized microstructure, we are interested in the following criteria:

- The synthetic microstructure must 'look like' the seed image. The similarity measures in this work come from the field of metallography/crystallography including lower order statistics (e.g. grain size distribution, orientation distribution function) and finer statistical features (e.g. grain boundary connectivity descriptors, higher order orientation correlations).
- Physical properties of the synthetic microstructure such as elastic moduli must be within reasonable bounds to the properties of the original microstructure. The properties were tested using finite element models and compared to experiments and bounding theories.

3.1. Example 1. Polycrystal

A polycrystalline structure with grayscale data from [22] was chosen for reconstruction. The free parameter in the reconstruction is the sampling window size which is taken to be $w = 13 \times 13$ pixels. To compare the sample image with reconstructed image, two global feature vectors were extracted from the input microstructure.

(1) Heyn's intercept histogram [23, 24] is employed for assessing the grain sizes. Histograms of the intercept length distribution (mean intercept length versus number of test lines possessing the mean intercept length) is used as the feature vector.
(2) Rose of intersections [25] is used as the feature vector for assessing grain shapes. To obtain the rose of intersections, a network of parallel equidistant lines is placed over the microstructure image at several angles and the number of grain boundary intersections with each test line is measured. The histogram of intersections with the angle of orientation of the lines is called the rose of intersection.

These features were compared with similar features from a few snapshots (with the same size as the input image) extracted from the reconstructed microstructure. Our results for case (1) (figure 4) look quite impressive. The MRF model is not only able to reconstruct the local features such as grain boundaries and connectivities, the global feature vectors (intercept histogram and rose of intersections) compare favorably with the input image.

3.1.1. Comparison of moment invariants. In this section, we compare descriptors that describe the shape distribution of individual grains in the experimental and synthesized grains in example 1, rather than the global (average) feature represented in the histograms of figure 4. Moment invariants (MIs) are non-linear combinations of moments of an object shape that are invariant with respect to a class of coordinate transformations [29]. For 1D distribution of data, the second order moment is analogous to standard deviation while the 4th order moment invariant is similar to kurtosis. For 2D shapes, DeGraef and coworkers [26–28] have identified 2 MI's (ω_1, ω_2) of second order, details about their values for various possible 2D shapes are given in [26]. Graphical representation for these two second order moment invariants in a x-y plot is known as second order moment invariant map (SOMIM). The SOMIM for the image in figure 5 and its reconstruction using MRFs is shown in figure 6. To compare the SOMIMs, we need to introduce an appropriate similarity metric. The modified Bhattacharya coefficient $H(p, q)$, also known as Hellinger distance, provides a metric to distinguish between two different density maps p and q. The regular Bhattacharya coefficient $\beta(p, q)$ is a measure of the similarity between two normalized distributions and can be written in discrete form as [30, 31]

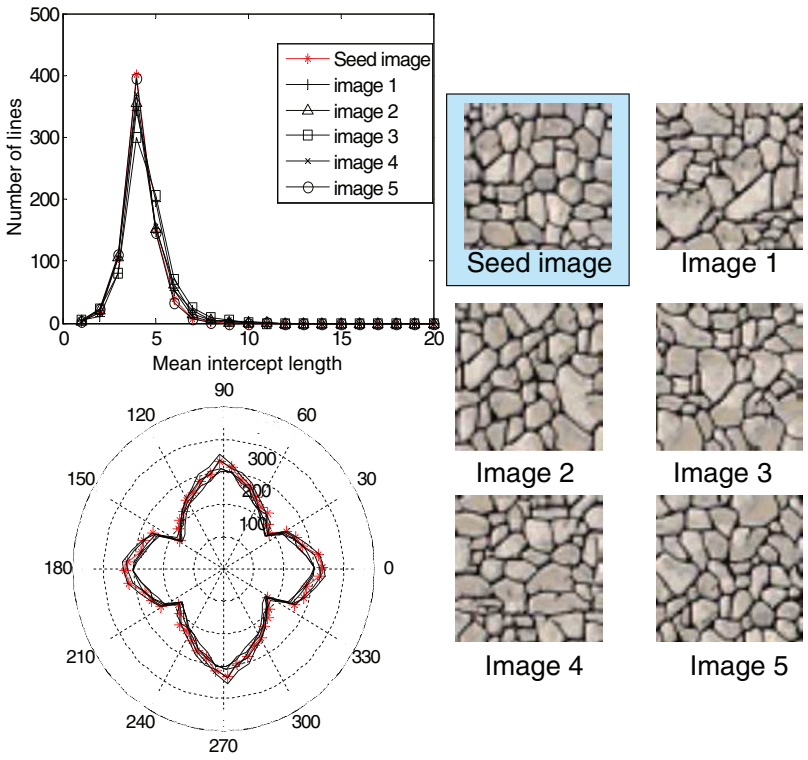

Figure 4. Statistics of synthesized images are compared with the seed image. The mean intercept length and rose of intersections are shown. Note that none of the synthesized images are identical to the seed image, yet global statistics of the seed image are well captured.

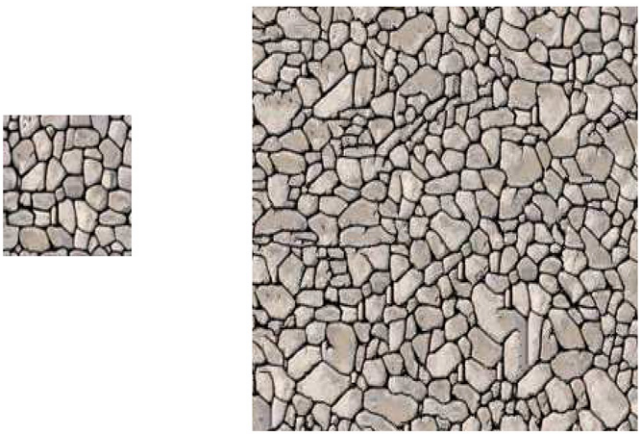

Figure 5. Initial microstructure (left) and the synthesized microstructure (right) from our Markov random field code. Note that local features such as grain boundaries are effectively captured.

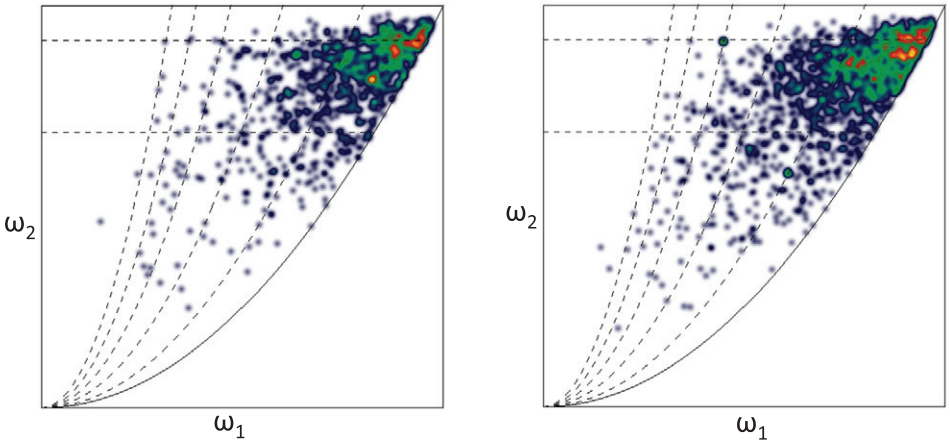

Figure 6. SOMIM density map original (left) and synthetic (right) microstructure.

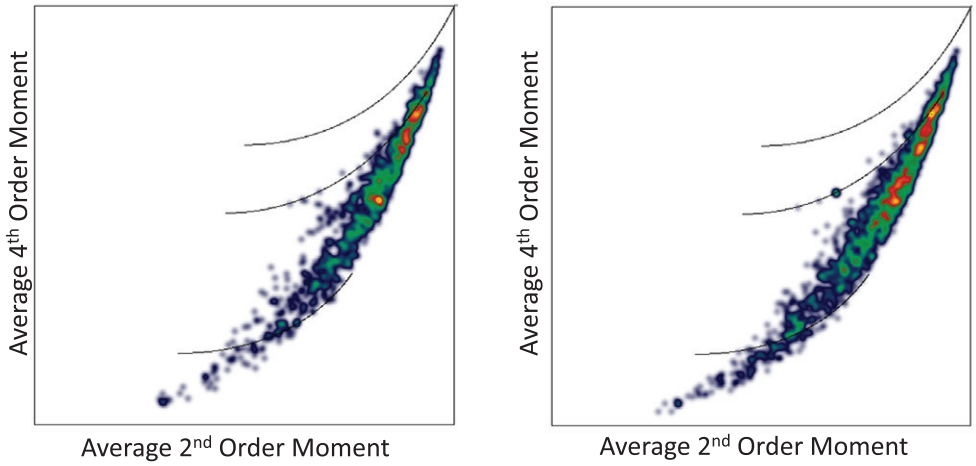

Figure 7. PMIM density map original (left) and synthetic (right).

$$\beta(p,q) = \sum_{i=1}^{N} \sqrt{p(i)q(i)}, \left(\text{with } \sum_{i=1}^{N} p(i) = \sum_{i=1}^{N} q(i) = 1 \right) \tag{3}$$

where the summation runs over the N bins of the SOMIM. The larger the value of β, more similar the two distributions are. The Hellinger distance $H(p, q)$ is defined by [32] as

$$H(p,q) = \sqrt{1 - \beta(p,q)} \tag{4}$$

Value of H for SOMIM is 0.47 for the polycrystalline case in example 1. This value indicates good reproduction of polycrystalline shapes using the MRF synthesis approach.

Alternately, a shape descriptor called projected moment invariant maps(PMIM) can also be plotted for the individual grains [26]. In this plot, averaged MIs of second through fourth order are plotted graphically in 2D or 3D plots. To make a comparison of synthesized with

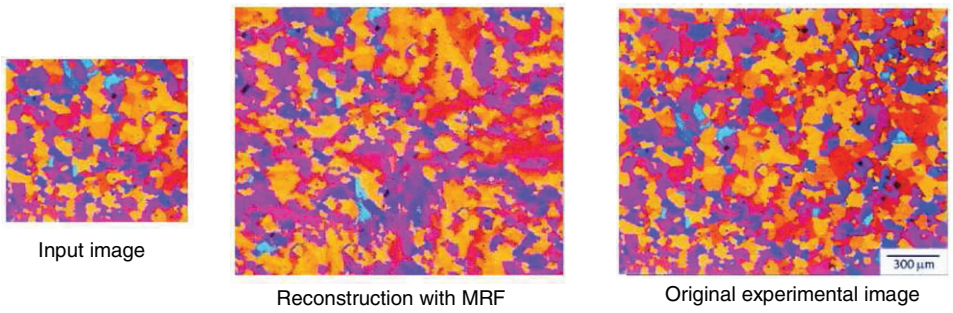

Figure 8. Reconstruction of an experimentally measured AA3002 Aluminum alloy microstructure [33] using Markov random Field algorithm. (a) Input micrograph (b) MRF reconstruction Purple regions are cube/near cube grain orientations, yellow/red regions are non-cube orientations. The fine dark spots are the intermetallic phases. (c) The larger microstructure from which the input image is taken is also shown for comparison.

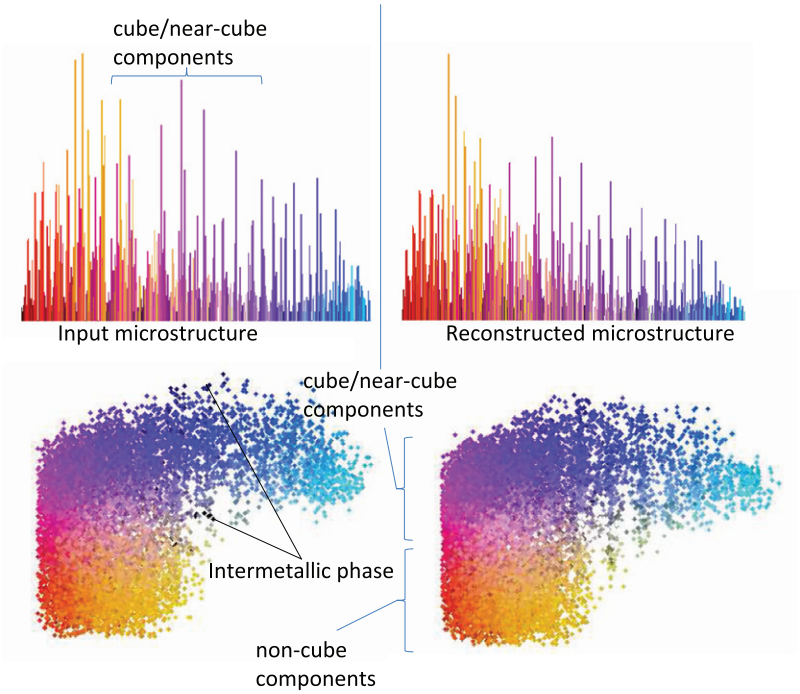

Figure 9. Color histograms of the input microstructure and reconstructed microstructure are compared. A novel color blot method is used to compare the distribution of cube/near cube regions, and intermetallic phases in the input and synthesized images.

original image, we used combination of second and fourth order moments in a 2D PMIM. The density maps for PMIM for the original and reconstructed image are compared in figure 6. The Hellinger distance of PMIM is 0.37, again indicating a good reconstruction.

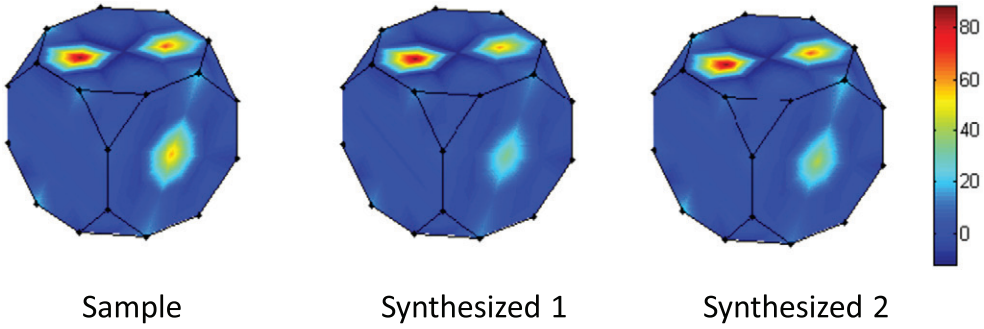

Figure 10. ODFs of sample micrograph is compared with the two synthesized images.

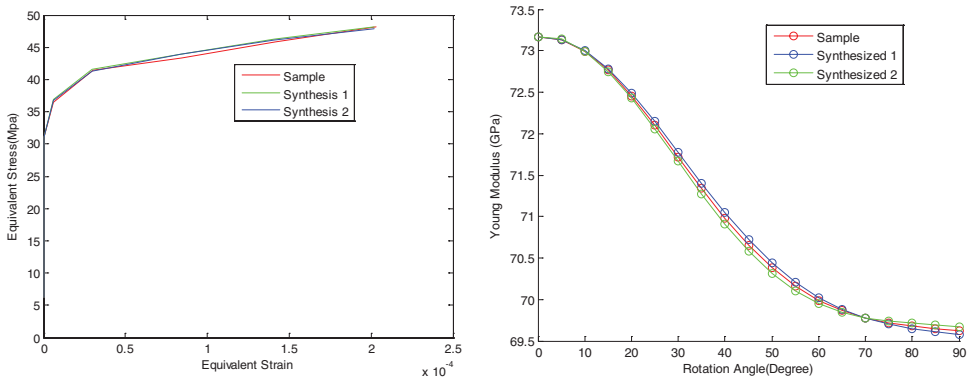

(a) (b)

Figure 11. (left) Comparison of the equivalent stress–strain curve predicted through homogenization for sample and two synthesized image (right) Variation of Young's Modulus with angle of rotation for sample and synthesized images.

3.2. Example 2. Aluminum alloy AA3002 representing the rolling plane

In the second example, microstructure of the Aluminum alloy AA3002 measured using polarised light microscopy [33] was used. The microstructure represents the rolling plane and reveals a fully recrystallised grain structure with randomly distributed intermetallic phases (dark spots in the image). The microstructure is colored based on the occurrence of near-cube and non-cube orientations. This analysis is based on observed contrast effects when the object is rotated relative to the polarised light directions. Purple regions are cube or near-cube orientations, whereas the yellow/red regions are non-cube. The Markov random field reconstruction and the original microstructure are indicated in figure 8. Only a small part (in figure 8(a)) of the larger experimental image (in figure 8(c)) was used for the reconstruction and the reconstructed image of larger size (in figure 8(b)) was compared with the larger experimental image. The microstructure was reconstructed using a 150×170 pixel input image shown in figure 8 (left) using a window size of $w = 7 \times 7$ pixels. The fraction of cube versus non-cube orientations and distribution of intermetallic phases was studied using color histograms and color clouds. The color cloud used here is an attempt at showing the pixels in 'color space' rather than Euclidean space ('microstructure'). Color densities are converted into scattered

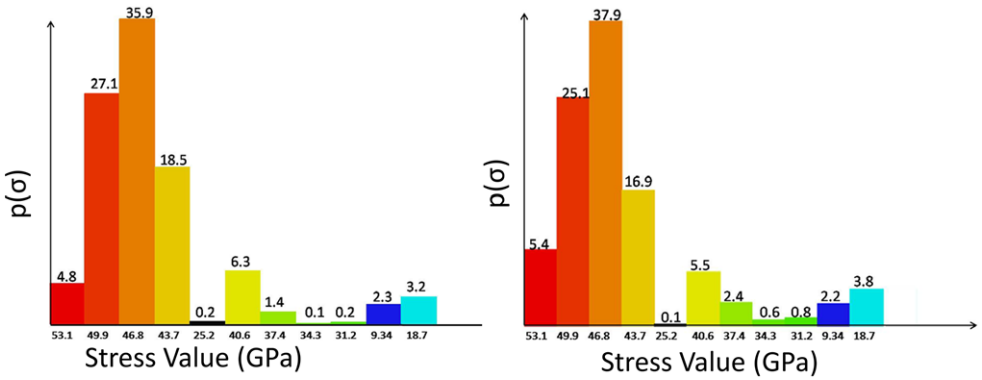

Figure 12. Comparison of the distribution of the equivalent stress in a finite element simulation using a color histogram (left) Experimental image (right) Synthesized image 1.

random dots around the spatial position assigned to the color, with the extent of the spatial position determined by the frequency with which that RGB triplet appears in the image.

The color blot and color histogram results shown in figure 9 show good visual correlation of the reconstructed image with the experimental input image. The texture components (cube versus non-cube orientations) are well reproduced in the larger synthesized image.

3.2.1. Comparison of microstructure sensitive properties. We performed finite element calculations on synthesized and sample image in figure 8 and compared the Young's Modulus with angle of rotation for sample and synthesized image. The calculations were based on a crystal plasticity model for Aluminum (from [34]) and was performed at a constant strain rate of 6.667×10^{-4} s^{-1} and a temperature of 300 K. To measure the statistically similarity between sample and synthesized image, we calculated the orientation distribution function(ODF) by assigning a unique orientation to each pixel based on its color. In figure 10 we have shown ODF for sample and two synthesized images and we observed that ODF for synthesized images is very close to that of sample image. In figure 11(b), we have plotted the variation of Young's Modulus (E) with sample rotation angle for the original and reconstructed images. In figure 11(a) we have plotted the equivalent stress-strain response for sample and synthesized image for a shear test. We also compared the stress histograms for the original and reconstructed image. The histogram plots the number of pixels in the microstructure within a given stress range. The color histogram of stresses shown in figure 12 reveal that the global response of the synthesized image is very similar to that of sample microstructure.

4. Conclusions

It is human intuition that different windows taken from a polycrystalline microstructure generally 'look alike'. This can be quantified through an underlying stationary probability distribution that generates all possible microstructural windows. While quantifying this high dimensional joint probability distribution of all pixel colors is computationally intractable, we looked at sampling methods to model this distribution. For many microstructures, the probability of a pixel color depends only on the pixel state of its close neighbors. Thus, one could represent microstructures in the form of undirected probabilistic graphs called Markov random fields (MRFs) with pixels interacting with neighbors over a sampling window.

With this lattice structure, we employed a sampling algorithm to compute the conditional probability density for the state of each pixel given the known states of its neighboring pixels. In the implementation, the microstructure is grown layer-by-layer from a small seed image (3×3 pixels) taken randomly from the sample. To synthesize a pixel, the algorithm first finds all windows in the sample image that are similar to the unknown pixel's neighborhood window. One of these matching windows is chosen and its center pixel is taken to be the newly synthesized pixel. We have artificially synthesized 2D polycrystalline microstructures using the sampled probabilities. Previous methods for reconstructing polycrystals using algorithms based on a common set of underlying features such as marginal histograms and point probability functions have often failed to capture the local information such as sharp grain boundaries. We find that the MRF approach is an attractive solution in this regard.

We show that not only are the global features such as grain size/shape distribution captured but the localized grain features such as shape moments also closely match with those of the experimental images. In addition, the texture distribution and mechanical (elastic) properties of the synthesized microstructures as computed using finite element method were also found to closely reproduce the experimental values. Finally, we plotted the stress histograms from a finite element test and these were also well reproduced. Our results evidence to the notion of a stationary probability distribution underlying microstructure formation. Future efforts will aim to analytically model such a distribution by using high dimensional regression to fit the results of the sampling algorithm. In addition, it will be of interest to use this tool to study the temporal evolution of such a distribution during microstructure evolution.

Acknowledgments

The work presented here was funded by Air Force Office of Scientific Research (AFOSR) grant number FA9550-12-1-0475 and FA9550-12-1-0458

References

[1] Heeger D J and Bergen J R 1995 Pyramid-based texture analysis/synthesis *SIGGRAPH* pp 229–38
[2] Bonet J S D 1997 Multiresolution sampling procedure for analysis and synthesis of texture images *SIGGRAPH* pp 361–8
[3] Simoncelli E P and Portilla J 1998 Texture characterization via joint statistics of wavelet coefficient magnitudes *Proc. 5th Int. Conf. on Image Processing (Chicago, IL, 1998)*
[4] Torquato S 2002 *Random Heterogeneous Materials: Microstructure and Macroscopic Properties* (New York: Springer)
[5] Yeong C L Y and Torquato S 1998 Reconstructing random media *Phys. Rev.* E **57** 495–506
[6] Lee H, Brandyberry M, Tudor A and Matos K 2009 Three-dimensional reconstruction of statistically optimal unit cells of polydisperse particulate composites from microtomography *Phys. Rev.* E **80** 061301
[7] Popat K and Picard R 1993 Novel cluster-based probability model for texture synthesis, classification, and compression *Visual Communications and Image Processing* pp 756–68
[8] Zhu S, Wu Y and Mumford D 1998 Filters, Random fields and maximun entropy (FRAME)—towards a unified theory for texture modeling *Int. J. Comput. Vis.* **27** 107–26
[9] Paget R and Longstaff I 1998 Texture synthesis via a noncausal nonparametric multiscale Markov random field *IEEE Trans. Image Process.* **7** 925–31
[10] Efros A and Leung T 1999 Texture synthesis by non-parametric sampling *Int. Conf. on Computer Vision* vol **2** pp 1033–8
[11] Ising E 1925 Beitrag zur Theorie des Ferromagnetismus *Z. Phys.* **31** 253–8
[12] Grigoriu M 2010 Nearest neighbor probabilistic model for aluminum polycrystals *J. Eng. Mech.* **136** 821–9

[13] Shannon C E 1948 A mathematical theory of communication *Bell Syst. Tech. J.* **27** 379–423
[14] Sundararaghavan V 2014 Reconstruction of three dimensional anisotropic microstructures from two-dimensional micrographs imaged on orthogonal planes *Integr. Mater. Manuf. Innov.* **3** 19
[15] Zhang K S, Wu M S and Feng R 2005 Simulation of microplasticity-induced deformation in uniaxially strained ceramics by 3D Voronoi polycrystal modeling *Int. J. Plast.* **21** 801–34
[16] Lebensohn R A, Castelnau O, Brenner R and Gilormini P 2005 Study of the antiplane deformation of linear 2D polycrystals with different microstructures *Int. J. Solids Struct.* **42** 5441–59
[17] Watanabe O, Zbib H M and Takenouchi E 1998 Crystal plasticity: micro-shear banding in polycrystals using voronoi tessellation *Int. J. Plast.* **14** 771–88
[18] Brahme A, Alvi M H, Saylor D, Fridy J and Rollett A D 2006 3D reconstruction of microstructure in a commercial purity aluminum *Scr. Mater.* **55** 75–80
[19] Besag J 1974 Spatial interaction and the statistical analysis of lattice systems *J. R. Stat. Soc.* B **36** 192–236
[20] Wei L-Y, Lefebvre S, Kwatra V and Turk G 2009 State of the art in example-based texture synthesis *EUROGRAPHICS* State of the Art Report EG-STAR 93–117
[21] Umekawa S, Kotfila R and Sherby O D 1965 Elastic properties of a tungsten-silver composite above and below the melting point of silver *J. Mech. Phys. Solids* **13** 229–30
[22] Lefebvre S 2006 Hoppe H.: appearance-space texture synthesis *SIGGRAPH* pp 541–8
[23] Vander Voort G F 1993 Examination of some grain size measurement problems *Metallography: Past, Present and Future (75th Anniversary Volume) ASTM STP 1165* (Philadelphia: American Society for Testing and Materials) p 266
[24] Vander Voort G F 1984 *Metallography: Principles and Practice* (New York: McGraw-Hill)
[25] Saltykov S A 1974 *Stereometrische Metallographie* (Leipzig: Deutscher Verlag fur Grundstoffindustrie)
[26] Callahan P G, Simmons J P and De Graef M 2012 A quantitative description of the morphological aspects of materials structures suitable for quantitative comparisons of 3D microstructures *Modelling Simul. Mater. Sci. Eng.* **20** 34–43
[27] MacSleyne J P, Simmons J P and De Graef M 2008 On the use of moment invariants for the automated analysis of 3D particle shapes *Modelling Simul. Mater. Sci. Eng.* **16** 045008
[28] MacSleyne J P, Simmons J P and De Graef M 2008 On the use of 2D moment invariants for the automated classification of particle shapes *Acta Mater.* **56** 427–37
[29] Hu M K 1962 Visual pattern recognition by moment invariantsIRE *Trans. Inf. Theory* **8** 179–87
[30] Bhattacharyya A 1946 On a measure of divergence between two statistical populations defined by their probability distribution *Ind. J Stat.* **7** 402–6
[31] Aherne F, Thacker N and Rockett P 1997 The Bhattacharyya metric as an absolute similarity measure for frequency coded data *Kybernetika* **32** 1–7
[32] Comaniciu D, Ramesh V and Meer P 2003 Kernel-based object tracking *IEEE Trans. Pattern Anal. Mach. Intell.* **25** 564–77
[33] Wittridge N J and Knutsen R D 1999 A microtexture based analysis of the surface roughening behaviour of an aluminium alloy during tensile deformation *Mater. Sci. Eng.* A **269** 205–16
[34] Sundararaghavan V and Zabaras N 2006 Design of microstructure-sensitive properties in elasto-viscoplastic polycrystals using multi-scale homogenization *Int. J. Plast.* **22** 1799–824